
Proceedings Paper:
Bokhove, O., Bolton, J. and Thompson, H. (2024) Geometric power optimisation of a rogue-wave energy device in a (breakwater) contraction. In: 2024 IEEE Conference on Control Technology and Applications (CCTA). 8th IEEE Conference on Control Technology and Applications (CCTA 2024), 21-23 Aug 2024, Newcastle Upon Tyne, UK. IEEE. ISBN: 979-8-3503-7095-9. ISSN: 2768-0762. EISSN: 2768-0770.

https://doi.org/10.1109/CCTA60707.2024.10666543

Geometric power optimisation of a rogue-wave energy device in a (breakwater) contraction

Onno Bokhove[1], Jonny Bolton[1], and Harvey Thompson[2]

***Abstract*— A comprehensive mathematical model is developed for a wave energy device placed in a contraction coupled to a tubular generator with more than one induction coil. The model is used to maximize the power output from the device as a function of two contraction geometry parameters and the average water depth. It is shown that increasing the number of induction coils is highly beneficial and that moving from one to three induction coils can increase the power output from the device by an order of magnitude.**

I. INTRODUCTION

There are a wide variety of devices that can harness wave energy, which can be placed in specific locations such as in the open ocean, in coastal waters or on the coast. We consider a niche wave energy device that is perhaps best embedded as part of the coastline, in particular either on a larger scale in a breakwater or on a smaller scale as part of a dock. The device consists of a buoy shaped and fit to move uni-directionally with and against gravity in a contraction. This contraction is used to enhance the wave action onto a buoy which is in turn driving a tubular permanent-magnet power generator. The device combines features of the tapered channel or Tapchan device (in which waves are raised to spill into a higher reservoir), heaving wave buoys with a linear and vertically-aligned generator, and the oscillating water column (OWC) driving Wells' wind turbines placed in a breakwater or on the open sea [10]. In the absence of the contraction and movement along a vertical wall, our device resembles the Berkeley wedge wave device [13] but that device has a sliding rail and sliding non-tubular linear motor. Alternatively, our device can be placed in a floating contraction geometry at sea, as in the device of Yu et al. [16], in which a contraction geometry is used to enhance the forces on 2×2 OWCs on its slanted side walls. The advantage of our device is the direct conversion of wave energy via buoy motion into electrical power. Our device was inspired by the rogue-wave amplification in the "bore-soliton-splash" [5].

A rendering of the device is given in Fig. 1. The dynamics involved has three integrated aspects: the waves coming from the sea enter the contraction, wherein a buoy is moving uni-directionally, and a main magnet attached to this buoy travels through tubular coils to generate the energy. A complete wave-to-wire mathematical model has been derived and partially explored in a series of papers [5], [6], [7]. Particular in that derivation is that the entire conservative part of the model can be derived from one variational principle, with embedded therein the full two-way couplings between wave dynamics and buoy motion as well as integrated buoy motion and tubular electromagnetic power generation. The latter buoy-generator integration involves an analytic reduction of the three-dimensional Maxwell's partial differential equations in a symmetric, cylindrical configuration to two ordinary differential equations for the dynamics of charge and current in a single induction coil. Whereas the wave dynamics was modelled with nonlinear potential flow or Boussinesq-type partial differential equations and the buoy motion by two ordinary equations for the position and speed of the buoy. The advantage of this Boussinesq-type wave modelling over Navier-Stokes hydrodynamics is its speed and accuracy for the fast inertial wave motions involved. Such approximations are well-explored and customary in the wave dynamics community but have barely been explored in conjunction with (the optimisation of) wave-energy devices. Preliminary numerical investigations were undertaken by us based on a linear shallow-water version of this full wave-to-wire model. Here our aim is to optimise the power output of the device.

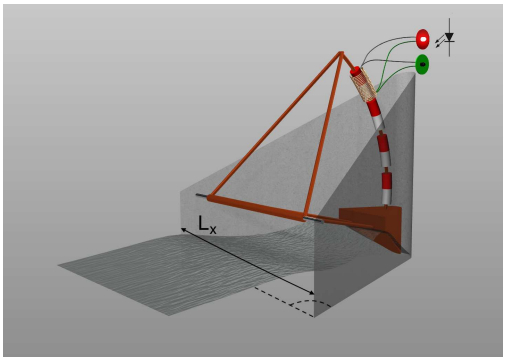

(a) Rendering of device in contraction with PTO, loads and incoming waves with motion along an arc (courtesy Wout Zweers). L_x and angle (dashed curve) θ_c indicated.

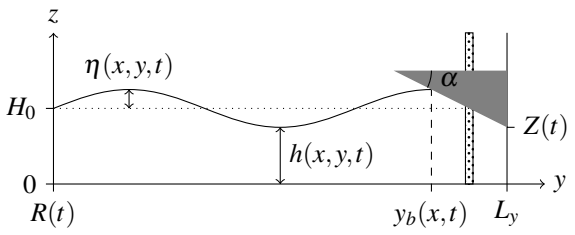

(b) Side view with buoy constrained to move vertically.

Fig. 1: Sketch of the wave-energy device (taken from [7]).

[1]OB & JB, Leeds Institute of Fluid Dynamics, University of Leeds, LS2 9JT, Leeds, UK o.bokhove@leeds.ac.uk

[2]HT, School of Mechanical Engineering, University of Leeds, UK h.m.thompson@leeds.ac.uk

This paper explores two approaches to increasing the power output from the wave-energy device. The first develops a theoretical formulation of the tubular generator with more than one induction coil. Tubular generators have several advantages (e.g. direct conversion) and disadvantages (e.g. requiring robust ball-bearings for motion guidance), for a discussion see [4], [12]. The benefits of using three induction coils instead of one are explored in detail. The second approach is based on surrogate-enabled optimisation where the design variables are the width and angles of the linear buoy and contraction geometry. Linear finite-element modelling (§III) of the entire device is carried at a set of Design-of-Experiment points based on Latin-hypercube-sampling. An overview of such geometric optimisation is given in [11].

II. WAVE-TO-WIRE MATHEMATICAL MODEL: BUOY AND GNERATOR

While we refer to Bokhove, Kalogirou and Zweers [5] for the full, original derivation of the wave-to-wire model, we will here focus on consequences of an extension in the set-up of the tubular generator with its connection to the buoy motion[1]. The unidirectional motion of the buoy is governed by its vertical position $Z(t)$, its velocity $W(t) = \dot{Z} \equiv \mathrm{d}Z/\mathrm{d}t$ under gravity with acceleration g downwards, the hydrodynamic force $F(t)$ on its hull and the forces due to the electromagnetic drag. The buoy with its mast and magnet has mass M and is constrained to move vertically[2].

The extension consists of replacing the single induction coil of length L with three induction coils each of length $L/3$ with reoriented winding configurations followed by an (ideal) full-phase AC-DC full-bridge rectifier for each coil. Note that this choice is purely for illustrative purposes and the model can, in principle, be extended to any number of induction coils. Each rectifier takes care that the alternating current I_i in coil i becomes a DC-current $|I_i|$ with $i = 1,2,3$, which set-up is somewhat related to work in [3]. The length L_m of the single magnet stays the same. Those DC currents in the model are directly used in a Shockley equation representing energy-consuming LED loads since the coils are mathematically connected in parallel via the Shockley equation. Each induction circuit has charge $I_i = \dot{Q}_i$ with the dot denoting a time derivative.

Consequently, the coupled dynamics of the buoy and tubular motor with a single magnet moving through the three induction coils consists of eight ordinary differential equations, as follows

$$\dot{Z} = W, \tag{1a}$$

$$M\dot{W} = -Mg - 2\pi a \sum_{i=1}^{3} \varepsilon_I^{(i)}(Z) I_i + F, \tag{1b}$$

$$\dot{Q}_i = I_i, \tag{1c}$$

$$L_i^{(i)} \dot{I}_i = 2\pi a \varepsilon_I^{(i)}(Z)\dot{Z} - (R_i^{(i)} + R_c^{(i)}) I_i - \frac{I_i}{|I_i|} V_S(|I_1| + |I_2| + |I_3|) \tag{1d}$$

for $i = 1,2,3$, with coil densities $\varepsilon_I^{(i)}(Z)$ (see below), a Shockley equation

$$V_S(|I|) = n_q V_T \ln(1 + |I|/I_{sat}) \quad \text{with } |I| = |I_1| + |I_2| + |I_3|, \tag{1e}$$

n_q a quality factor, V_T a thermal voltage and I_{sat} a saturation current. The energy is consumed in loads modelled by a Shockley equation after these AC-DC rectifications. The load is partitioned mathematically into each equation via the overall rectified current $|I| = |I_1| + |I_2| + |I_3|$, which is argued to be the case by the following argument, supported by the circuit diagram in Fig. 2.

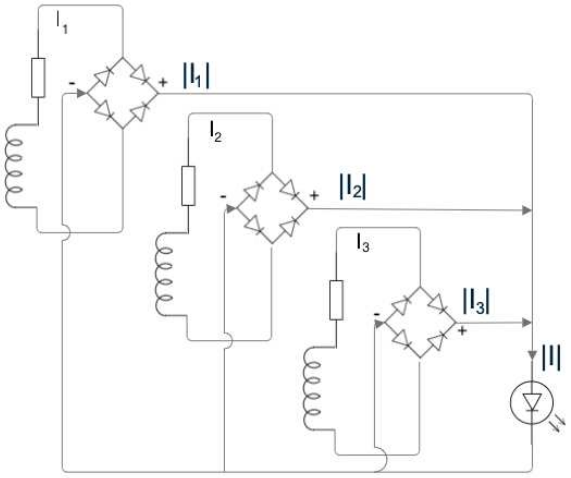

Fig. 2: Circuit schematic of three induction coils, each with inductance $L_i^{(i)} = L_i/3$, resistance of induction coil and its circuit $R_c^{(i)} + R_i^{(i)} = (R_c + R_i)/3$, in which each AC-current I_i is rectified to a DC current $|I_i|$ for $i = 1,2,3$, and connected in parallel to a Shockley load, pictured as light-emitting LED.

Consider the case where I_1, I_2, I_3 all have the same signs, then the voltage drop V_s is the same for each induction equation and V_s has $I = |I_1 + I_2 + I_3|$ as argument. The coil densities are nonlinear functions of buoy position Z and are approximately given by a modification of expression (44e)

[1]We are particularly building on the model derivation of a tubular generator with a single magnet and single induction coil in the Appendix of Bokhove, Kalogirou and Zweers [5]. However, we do note that the complete model is given here in the combined equation sets (1) and (9).

[2]Parameters and values/ranges used are found in Table I.

in [5], i.e. they take the forms

$$\varepsilon_I^{(1)}(Z) = \frac{a\mu N}{L}\Big(\frac{1}{(a^2+(\bar{Z}+\alpha_h H_m - Z - L/2)^2)^{3/2}} - \frac{1}{(a^2+(\bar{Z}+\alpha_h H_m - Z - L/6)^2)^{3/2}}\Big) \quad (2a)$$

$$\varepsilon_I^{(2)}(Z) = \frac{a\mu N}{L}\Big(\frac{1}{(a^2+(\bar{Z}+\alpha_h H_m - Z - L/6)^2)^{3/2}} - \frac{1}{(a^2+(\bar{Z}+\alpha_h H_m - Z + L/6)^2)^{3/2}}\Big) \quad (2b)$$

$$\varepsilon_I^{(3)}(Z) = \frac{a\mu N}{L}\Big(\frac{1}{(a^2+(\bar{Z}+\alpha_h H_m - Z + L/6)^2)^{3/2}} - \frac{1}{(a^2+(\bar{Z}+\alpha_h H_m - Z + L/2)^2)^{3/2}}\Big) \quad (2c)$$

for the three coils located after a centering shift at $[-L/2, L/6]$, $[-L/6, L/6]$ and $[L/6, L/2]$ instead of one coil located after this shift at $[-L/2, L/2]$. The single coil has N windings, radius a and length L, while the shorter coils each have $N/3$ windings and length $L/3$. The distance above the reference buoy position Z is $\alpha_h H_m$ and the rest level position of the buoy is $\bar{Z}$, with $\alpha \in [0,1]$.

TABLE I: Table with symbols, units and parameter values or ranges used throughout this paper.

Parameter	symbol	unit	value
tank width	L_x	m	$[0.2, 0.55]$
rest free-surface depth	H_0	m	$[0.075, 0.15]$
mass buoy	M	kg	0.08
mast length	H_m	m	0.2
one-coil length	L	m	0.025
current	I	A	
coil diameter	D	mm	0.2769
coil outer radius	a	m	0.012
winding layers	n_{li}	-	10
coil windings	$N = n_{li}L/D$	-	(2889)
magnetic dipole mom.	m	Am^2	5
magnet radius	A_m	m	0.0075
magnet length	L_m	m	0.025
scale factor	α_h	-	0.05
permeability	μ_0	H/m	$4\pi 10^{-7}$
magnetic flux	$\mu = \mu_0 m/(4\pi)$	Nm/A	
quality factor	K	-	0.53
coil induction	$L_i = K\pi a^2 \mu_0 N^2/L$	$\mathrm{NM/A}^2$	0.0099
conductivity	σ	A/VM	5.96×10^7
resistance coil	$R_c = 8aN/(\sigma D^2)$	V/A	18.97
resistance coil circuit	$R_i = R_c$	V/A	18.97
saturation current	I_{sat}	A	0.02
thermal voltage	V_T	V	2.05
Shockley quality factor	n_q	-	0.1
lin. Shockley resistance	$R_l = n_q V_T / I_{sat}$	V/A	102.5
acceleration of gravity	g	$\mathrm{m/s}^2$	9.81

Each induction coil with its rectifier acts as a "battery" unit. When these three units instead are placed in series there is only a single AC current I and DC (rectified) current $|I|$. We have explored the placement of the three AC-circuits in parallel after rectification and its altered formulation (1).

A. Resonance and Forced-Dissipative Analysis

The linearised coupled buoy-generator subsystem with one coil reads:

$$\dot{Z} = W, \quad (3a)$$

$$M\dot{W} = -\gamma G(Z_0) I + F(t), \quad (3b)$$

$$\dot{Q} = I, \quad (3c)$$

$$L_i \dot{I} = \gamma G(Z_0)\dot{Z} - (R_c + R_i + R_l) I - \frac{Q}{C}, \quad (3d)$$

in which we have added a capacitor C to the Shockley load with its linearised resistance R_l and in which the hydrodynamic forcing in the buoy's momentum equation is simplified to a prescribed force $F(t)$. The coil density $2\pi a \varepsilon(Z) \equiv \gamma G(Z)$ with $\gamma = 2\pi\mu a^2/L$ is evaluated at the rest level Z_0 of the buoy in the linearisation. The other variables have been linearised around their zero rest state. In the absence of forcing $F(t) = 0$ and dissipation $R_c = R_i = R_l = 0$, this subsystem of coupled oscillators has eigenfrequencies

$$\omega_i^2 = 0, \omega_i = \pm\sqrt{(L_i)^{-1}}\sqrt{1/C + \gamma^2 G(Z_0)^2/M} \quad (4)$$

with limiting cases $1/C \to 0$ and $\gamma \to 0$, in the latter which case $\omega_i \to \pm\sqrt{(L_i C)^{-1}}$. Hence, larger values of L_i, C, M reduce the eigenfrequency ω_i and larger values of $\gamma G(Z_0)$ and inverse capacitance $1/C$ increase the eigenfrequency. Regardless, adding a capacitor increases the eigenfrequency. Given that $\gamma = 2\pi a^2 \mu N/L$ and $L_i = K\mu_0 (N^2/L)\pi a^2$ ([5], [7]), it is best to look at the combination $\gamma^2 G(Z_0)^2/L_i$.

Next we analyse the subsystem (3) under harmonic forcing. Given that $F(t) \propto e^{i\sigma t}$, we posit solutions of the form

$$\begin{pmatrix} Z(t) \\ W(t) \\ I(t) \\ Q(t) \end{pmatrix} = \mathrm{Re}\left\{\mathbf{x} e^{i\sigma t}\right\} \equiv \mathrm{Re}\left\{ \begin{pmatrix} \hat{Z} \\ \hat{W} \\ \hat{I} \\ \hat{Q} \end{pmatrix} e^{i\sigma t} \right\},$$

such that, upon division by $e^{i\sigma t}$, system (3) can be written in matrix form as $\mathbf{A}\mathbf{x} = \mathbf{b}$, where

$$\mathbf{A} = \begin{pmatrix} i\sigma & -1 & 0 & 0 \\ 0 & iM\sigma & \gamma G & 0 \\ 0 & 0 & -1 & i\sigma \\ -i\gamma G\sigma & 0 & iL_i\sigma + R & \frac{1}{C} \end{pmatrix}$$

with $G \equiv G(Z_0)$ and $R \equiv R_c + R_i + R_l$, and

$$\mathbf{b} = (0, A_r + iA_i, 0, 0)^T.$$

The matrix $\mathbf{A}$ is inverted using Python's `sympy` package. To calculate the power, we do not require expressions for Z and W. We can explicitly evaluate the average power output, with $T = n\pi/\sigma$:

$$\hat{P}_g = \frac{1}{T}\int_0^T I^2 R_l + \frac{IQ}{C}\mathrm{d}t = \frac{1}{2}\Big(R_l\left(\mathrm{Re}\{\hat{I}\}^2 + \mathrm{Im}\{\hat{I}\}^2\right) + \frac{1}{C}\left(\mathrm{Re}\{\hat{I}\}\,\mathrm{Re}\{\hat{Q}\} + \mathrm{Im}\{\hat{I}\}\,\mathrm{Im}\{\hat{Q}\}\right)\Big), \quad (5)$$

since $\int_0^{n\pi/\sigma}\cos^2\sigma t \mathrm{d}t = \int_0^{n\pi/\sigma}\sin^2\sigma t \mathrm{d}t = n\pi/(2\sigma)$ and $\int_0^{n\pi/\sigma}\cos\sigma t \sin\sigma t = 0$. It can be shown that

$$\mathrm{Re}\{\hat{Q}\} = \mathrm{Im}\{\hat{I}\}/\sigma \text{ and } \mathrm{Im}\{\hat{Q}\} = -\mathrm{Re}\{\hat{I}\}/\sigma.$$

Hence, $\mathrm{Re}\{\hat{I}\}\mathrm{Re}\{\hat{Q}\}+\mathrm{Im}\{\hat{I}\}\mathrm{Im}\{\hat{Q}\}=0$, such that the second term of (5) can be removed, giving

$$\hat{P}_g = \frac{1}{2}R_l\left(\mathrm{Re}\{\hat{I}\}^2+\mathrm{Im}\{\hat{I}\}^2\right).$$

This yields

$$\hat{P}_g = \frac{1}{2}R_l C^2 G^2\gamma^2(A_r^2+A_i^2)/\left(\alpha_0^2+\alpha_1^2\right).$$

Substituting for α_0 and α_1 as well as dividing top and bottom by C^2, the final power output becomes

$$\hat{P}_g = \frac{1}{2}\frac{R_l G^2\gamma^2(A_r^2+A_i^2)}{\left(G^2\gamma^2-L_iM\sigma^2+M/C\right)^2+(MR\sigma)^2}. \tag{6}$$

At the resonance frequency $\gamma G(Z_0)/\sqrt{ML_i}\sim 0.2673$Hz (e.g. with $\gamma=3.66\times10^{-6}, M=0.1, L_i=0.35$, $R_l=102$, $R_i=R_c=203$, $\gamma G(Z_0)=0.05$) the power output is

$$\hat{P}_g = \frac{1}{2}R_l L_i(A_r^2+A_i^2)/(MR^2). \tag{7}$$

Therefore, with $R_l\approx 102$ and $A_r+iA_i=A$, one finds that $P\approx 7\times10^{-4}|A|^2=2.8\times10^{-7}$J for $A=0.02$.

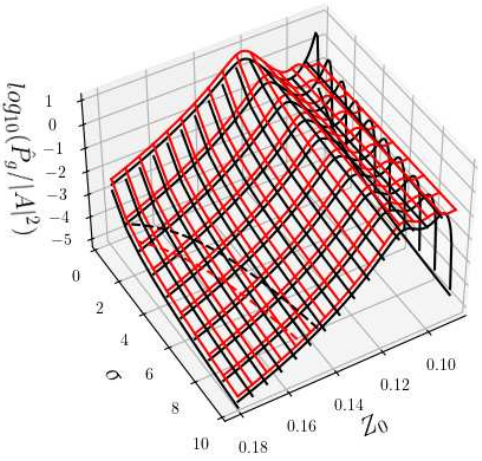

Fig. 3: Power output over amplitude $P_g/|A|^2$ as function of (modelled hydrodynamic) forcing frequency σ and buoy rest level Z_0 for single coil (black lines) and three-coils-in-parallel (red lines) cases, with full-wave rectifiers for each case. Resonant cases are displayed with dashed lines. Half of the profile is shown.

Similarly, the linearised forced-dissipative three-coil case connected in parallel after rectification involves eight equations, i.e. for $\{Z,W,I_1,Q_1,I_2,Q_2,I_3,Q_3\}$, and is approximated as follows

$$\dot{Z}=W, \tag{8a}$$
$$M\dot{W}=-\gamma G(Z_0)I+F(t), \tag{8b}$$
$$\dot{Q}_i=I_i, \tag{8c}$$
$$L_i\dot{I}_i=\gamma G_i(Z_0)\dot{Z}-(R_c^{(i)}+R_i^{(i)}+R_l)I_i \text{ for } i=1,2,3, \tag{8d}$$

in which R_l is the full linearised Shockley load, while we recall that $R_c^{(i)}=R_c/3, R_i^{(i)}=R_i/3$. Note that this is an approximation since a Shockley load has been included in each circuit because it is not clear how to linearise $-\mathrm{sign}(I_i)R_l(|I_1|+|I_2|+|I_3|)$. To allow another comparison between the single coil and three-coil cases, we have (also) increased the linearised Shockley load in the single-coil case by a factor of three: $R_l\to 3R_l, R\to R=R_c+R_i+3R_l$.

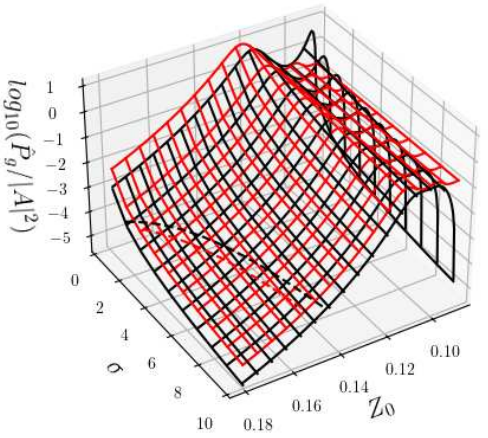

Fig. 4: Power output over amplitude $P_g/|A|^2$ as function of forcing frequency σ and buoy rest level Z_0 for single coil (black lines) and three-coils-in-parallel (red lines) cases, with full-wave rectifiers for each case. Resonant case displayed with dashed lines. Here we took $R_l\to 3R_l, R\to R_c+R_i+3R_l$ in the single-coil case.

Its solution for the currents without capacitor is also obtained using Python's `sympy` package. The power output for both the single coil and three-coil-in-parallel cases are displayed in Fig. 3 with solid black and red lines respectively as function of forcing frequency σ and (rest or linearisation) buoy level Z_0. The three-coil-in-parallel case reaches a higher power output of circa half a decade away from Z_0 with single-coil $G(Z_0)=0$. Near that point and for smaller σ the single-coil case is more effective. However, this difference is a bit artificial due to the associated linearisation process in that in reality Z marches through a range of values. Note that at resonance, the achievable maximally gained power is the same (7) between the one-coil and three-coil cases, as displayed with the dashed lines in Figs. 3 and 4. At least in the single-coil case, the effect of the capacitor control is minimal, since for $L_iM\sigma^2>\gamma^2G^2$ the term $(MR\sigma)^2$ dominates.

Of course, nonlinear effects will lead to some averaging over Z. A weakly nonlinear analysis or fully nonlinear numerical simulation will be required to assess the nonlinear effects of the coil densities and Shockley load.

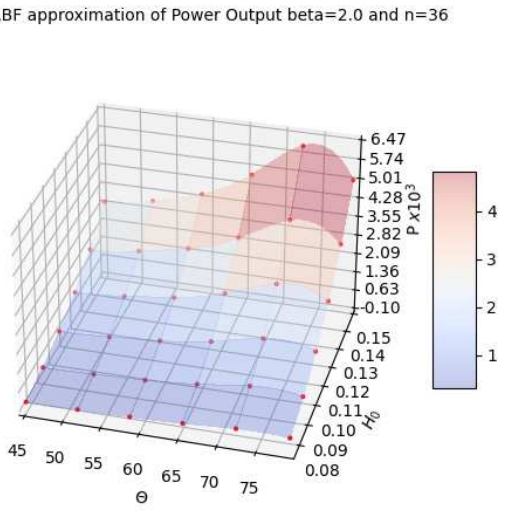

Fig. 5: Power output over 36 simulations with varying $\theta_c \in [45,80]^{\mathrm{o}}, H_0 \in [0.075,0.15]$m, while keeping $L_x = 0.2$m and other parameters fixed.

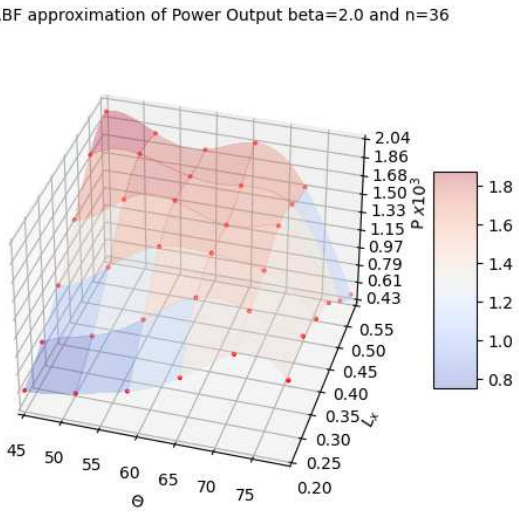

Fig. 6: Power output over 36 simulations with varying $\theta_c \in [45,80]^{\mathrm{o}}, L_x \in [0.2,0.55]$m, while keeping $H_0 = 0.1$m and other parameters fixed.

III. SURROGATE-ENABLED OPTIMISATION OF POWER OUTPUT: EFFECT OF CONTRACTION GEOMETRY

Hitherto we have chosen linear contraction and buoy geometries. The shape of the buoy is therefore a prism. The following three parameters determine contraction and buoy shapes: the width L_x of the contraction entrance, the angle $\theta = \theta_c$ of the contraction wall with the wall normal and the angle α of the buoy hull, see Fig. 1. Simulations of the linear shallow water finite-element model coupled to the buoy and then to the generator with loads will be used to calculate the power output for a series of parameter values. For details, we refer to [7] for our numerical set-up, which finite-element discretisation is fully compatible and includes two-way coupling between hydrodynamics and buoy motion as well as buoy motion and power generation[3]. Since a full sweep of simulations across a renewed set of parameter values over a regular grid pattern is computationally expensive, we also explore the use of surrogate modelling to lower the computational efforts. Here, we focus on the parameter plane spanned by θ_c and L_x or H_0 for incoming monochromatic waves, generated by a piston wavemaker for our laboratory-size tank. Unconstrained optimisation problems are solved where the goal is to find the parameter values that maximise the power output in order to aid in the design of the laboratory experiment. Two optimisation problems are considered where two of the three geometry parameters are varied and the third is fixed. For each case, surrogate models of power output are created using several sets of simulations.

In the first optimisation problem $L_x = 0.2$m is fixed and we calculate and display the power output for 36 value-pairings from Latin-hypercube sampling within parameter ranges $\theta_c \in [45,80]^{\mathrm{o}}, H_0 \in [0.075,0.15]$m. The second optimisation problem has $H_0 = 0.1$m fixed, and simulations are run for 36 value-pairings from Latin-hypercube sampling within parameter ranges $\theta_c \in [45,80]^{\mathrm{o}}, L_x \in [0.2,0.55]$m. Surrogate models of power output are created using Gaussian Radial Basis Functions, which will be used to find an overall fit and then to determine the maximum power output in each case. It turns out that a fitting with Gaussian Processes leads to unphysical negative power outputs so we rejected this choice of surrogate modelling.

The simulation sweep over θ_c and H_0 is displayed in Fig. 5, revealing a maximum power output of circa $\theta_c = 74^{\mathrm{o}}$ for all $H_0 \in [0.075,0.15]$m. Simulations (and surrogate modelling), displayed in Fig. 6, reveal maximum values of power output around a plateau bounded by lines connecting points $[74^{\mathrm{o}},0.2\mathrm{m}], [45^{\mathrm{o}},0.55\mathrm{m}]$ and $[74^{\mathrm{o}},0.2\mathrm{m}], [65^{\mathrm{o}},0.55\mathrm{m}]$ within the range $[\theta_c, L_x] = [45,80]^{\mathrm{o}} \times [0.2,0.55]$m investigated. Naturally, the power increases uniformly as function of H_0 since the piston wavemaker displacement stayed the same so more water is moved for larger H_0. Power should perhaps increase (linearly) with L_x which is, however, only seen for $\theta_c \in [45]^{\mathrm{o}}$, but there may be insufficient resolution within the contraction for large angle $\theta_c \approx 80^{\mathrm{o}}$.

IV. DISCUSSION

The optimisation studies carried out here have shown that the power output from a wave-energy device consisting of a wave-amplifying contraction and a floating buoy moving through a magnet can be increased significantly by replacing a single induction coil with three coils in parallel. The enhancement in power output is typically an order of magnitude for the three coil case and further studies are needed to investigate optimal multiple coil configurations. The optimisation

[3]Access to a bespoke GitHub repository is available upon request. More details of the calculations are found in [8].

studies have also shown that further significant improvements in power output can be achieved through careful selection of the wave-device's contraction geometry.

A fully nonlinear model was formulated in [5] in which the pressure under the wetted hull acts as a Lagrange multiplier $\tilde{\lambda} \geq 0$, with $\tilde{\lambda} = 0$ at the waterline. This waterline resides where water depth $z = h(x,y,t)$ equals the position of the buoy hull $z = h_b(Z(t),x,y)$ over a flat bed at $z = 0$. The waterline is defined by constraint $h(x,y,t) - h_b(Z(t),x,y) = 0$ with horizontal coordinates x and y and buoy location $Z(t)$. In h_b various parameters have been suppressed. This modelling requires meshes conforming to the dynamic waterline. Instead, we outline a formulation based on inequality constraints $h(x,y,t) - h_b(Z(t),x,y) \leq 0$, cf. developments of contact dynamics in continuum mechanics [9].

Consider a wavetank with piston wavemaker at $x = R_w(t)$ and a contraction such that $x \in [0,L_x], y \in [R_w(t), l_y(x)]$, with $l_y(x) = L_y - L_c|1 - 2x/L_x|$ and L_c the contraction length at the centreline, and $z \in [0,h(x,y,t)]$. At rest the water level in the tank is H_0 and under the buoy determined by Archimedes principle. A constant-density fluid with three-dimensional velocity $\mathbf{u} = \nabla\phi$ is governed by Laplace equation

$$\nabla^2\phi = 0 \tag{9a}$$

for velocity potential $\phi(x,y,z,t)$. Its time dependence is governed by kinematic and Bernoulli equations at $z = h(x,y,t)$:

$$\partial_t\phi + \frac{1}{2}|\nabla\phi|^2 + g(h - H_0) + F_+(\gamma_n(h - h_b) - \lambda) = 0, \tag{9b}$$

$$\partial_t h + \nabla\phi \cdot \nabla h = \partial_z\phi, \tag{9c}$$

coupled to the buoy motion via an added inequality constraint-force

$$M\dot{W} = -Mg - 2\pi a \sum_{i=1}^{3} \varepsilon_I^{(i)}(Z) I_i - \int_0^{L_x}\int_0^{l_y(x)} F_+(\gamma_n(h - h_b) - \lambda)\,\mathrm{d}x\,\mathrm{d}y, \tag{9d}$$

with $\partial_t h \equiv \partial h/\partial t, \partial_z\phi \equiv \partial\phi/\partial z, \nabla \equiv (\partial_x, \partial_y, \partial_z)^T$. The function $F_+(q) = \max(q,0)$, or a smooth approximation thereof, and Lagrange multiplier $\lambda(x,y,t)$ is the (negative) hydrodynamic pressure on the hull such that $\lambda \leq 0$ (N.B. $\tilde{\lambda} \propto -\lambda$)

$$\lambda = -F_+(\gamma_n(h - h_b) - \lambda), \tag{9e}$$

with constant $\gamma_n \gg 0$. One can show that (9e) for $F_+(q) = \max(q,0)$ satisfies the well-known Karush-Kuhn-Tucker inequality conditions $h - h_b \leq 0, \lambda \leq 0, \lambda(h - h_b) = 0$. So either $\lambda = 0$ or $h = h_b$. Lagrange multiplier equation (9e) and all (conservative parts of the) system can be derived from an augmented Lagrangian formulation (by combining work in [5], [14], [9]), aiding numerical formulation and implementation.

It is clear that full numerical simulations or weakly nonlinear analysis of the nonlinear (sub)-system of the device are required to further understanding. The benefits of adopting a model formulation for coupling the buoy based on an inequality constraint is currently being investigated within the finite-element environment `Firedrake` ([15], [1], [2], [14]). That environment in particular lends itself for the implementation of the (time-discrete) variational principle or augmented Lagrangian underlying the entire wave-to-wire model. Therein algebraically-complicated weak formulations can be generated automatically and the dissipative features can furthermore readily be added to these conservative parts. There is also an urgent need for experimental data for model validation, and the design and manufacture of a subsystem for experimental model validation is currently underway.

ACKNOWLEDGMENT

We acknowledge assistance from Duncan Borman in the built-up of this work [7]. JB's PhD, EPSRC Centre for Doctoral Training in Fluid Dynamics, University of Leeds, UK, funded by EPSRC grant EP/S022732/1.

REFERENCES

[1] M.S. Alnaes, UFL: a finite element form language. In: Automated Solution of Differential Equations by the Finite Element Method. Eds: A. Logg and K.-A. Mardal and G. N. Wells, Springer, Berlin. 2011.

[2] M.S. Alnaes, A. Logg, K.B. Oelgaard, M.E. Rognes, G.N. Wells G.N., Unified Form Language: A domain-specific language for weak formulations of partial differential equations. 2013. https://arxiv.org/pdf/1211.4047.pdf

[3] M. Baumann, J.W. Kolnar, Parallel connection of two three-phase three-switch buck-type unity-power-factor rectifier systems with DC-link current balancing. IEEE Trans. Industrial Electronics 54, 2007, 3042.

[4] N. Bianchi, S. Bolognano, D.D. Corte, F. Tonel, Tubular linear permanent magnet motors: an overall comparison. IEEE Trans. Industrial Applications 39(2), 2003, 0093-9994.

[5] O. Bokhove, A. Kalogirou, W. Zweers, From bore-soliton-splash to a new wave-to-wire wave-energy model. Water Waves 1(2), 2019, 217–258. For the movie of the man-made rogue wave, see: https://www.youtube.com/watch?v=YSXsXNX4zW0

[6] O. Bokhove, A. Kalogirou, D. Henry, G. Thomas, A novel rogue-wave-energy device with wave amplification and induction actuator. Int. Marine Energy Journal 30, 2020, 37–43.

[7] J. Bolton, O.Bokhove, D. Borman, A. Kalogirou, H. Thompson, Towards optimization of a wave-to-wire energy device in a breakwater contraction. European Wave and Tidal Energy Conf., Plymouth, 2021 10 pp. https://tethys-engineering.pnnl.gov/sites/default/files/publications/2191.pdf

[8] O. Bokhove, H. Thompson, Power optimisation of a rogue-wave energy device in a contraction. EarthArXiv https://eartharxiv.org/repository/view/7260/, 2024, 8 pp.

[9] E. Burman, P. Hansbo, M.G. Larson, The augmented Lagrangian method as a framework for stabilised methods in computational mechanics. Archives of Computational Methods in Engineering 30, 2023, 2579—2604.

[10] A.F.O. Falcäo, Wave energy utilization: a review of the technologies. Renew. Sustain. Energy Rev. 14, 2010, 899—918.

[11] A. Garcia Teruel, D.R. Forehand, Review of geometry optimisation of wave energy converters. Renewable and Sustainable Energy Reviews 139, 2021, 110593.

[12] P. Khatri, X. Wang, Comprehensive review of a linear electrical generator for ocean wave energy conversion. IET Renewable Power Generation 14, 2020, 949–958.

[13] F. Madhi, R.W. Yeung, On survivability of asymmetric wave-energy converters in extreme waves. Renew. Energy 119, 2018, 891—909.

[14] S. Balay, et al., PETSc, Toolkit for Advanced Optimisation: optimisation solvers, bound-constraint optimisation. 2023.

[15] F. Rathgeber et al., Firedrake: automating the finite element method by composing abstractions. ACM Trans. Math. Softw. 43(3), 2016, 27.

[16] T. Yu, Q. Guo, H. Shi, T. Li, X. Meng, S. He, et al. Experimental investigation of a novel OWC wave energy converter. Ocean Eng. 257, 111567. 2022.